# *Recent developments in nanostructured materials for high-performance thermoelectrics*

Article

Accepted Version

# Recent Developments in Nanostructured Materials for High-Performance Thermoelectrics

**Paz Vaqueiro*** **and Anthony V Powell**

**Department of Chemistry &**

**Centre for Advanced Energy Storage and Recovery (*CAESAR*),**

**Heriot-Watt University**

**Edinburgh EH14 4AS UK**

*Author for correspondence:
Dr P. Vaqueiro
Department of Chemistry
Heriot-Watt University
Edinburgh EH14 4AS
UK
Fax: +44 (0)131 451 3180
E-mail: chepv@hw.ac.uk

**Abstract**

This highlight discusses recent trends in the search for new high-efficiency thermoelectric materials. Thermoelectric materials offer considerable attractions in the pursuit of a more efficient use of existing energy resources, as they may be used to construct power-generation devices that allow useful electrical power to be extracted from otherwise waste heat. Here, we focus on the significant enhancements in thermoelectric performance that have been achieved through nanostructuring. The principal factor behind the improved performance appears to be increased phonon scattering at interfaces. This results in a substantial reduction in the lattice contribution to thermal conductivity, a low value of which is a key requirement for improved thermoelectric performance.

## Introduction

Global energy consumption, currently of the order of 14 TW, is predicted to increase by 44% between 2006 and 2030, with the strongest growth taking place in emerging economies.[1] The majority of this energy demand is satisfied by burning fossil fuels, which has concomitant problems associated with the emission of greenhouse gases. The combination of declining fossil fuel reserves and climate change arising from increased $CO_2$ emissions pose a challenge to society on a global scale.[2] Whilst fiscal and legislative measures may have a short-term impact, technology offers the only realistic hope for a long term solution, through the development of new energy carriers, alternative energy generation techniques, including renewable sources and advanced energy recovery methods to permit more efficient use of existing resources. This has led to a tremendous increase in research directed towards materials for energy applications including those for improved batteries,[3] fuel cells,[4] hydrogen storage systems, [3] photovoltaic applications,[5] supercapacitors[3] and thermoelectric devices. Thermoelectric devices in particular offer opportunities to achieve significant efficiency savings using current power-generation technologies: a key factor given the likely lead times for implementation of techniques utilizing novel energy carriers or generation from renewables. Efficiency savings are of particular importance for those regions, including Europe, in which non-renewable energy reserves (oil, coal, uranium) are relatively scarce, and thus making best possible use of available energy resources is essential for sustainability.

A thermoelectric device is a solid-state energy converter that transforms heat directly into electricity. It comprises an array of *n*- and *p*-type semiconducting materials (Figure 1). When a temperature difference is applied across the ends of an *n*-/*p*-couple, the working fluid of electrons and holes diffuses, creating an electric field and establishing an electrochemical potential. This potential can drive a current in an external circuit and thus perform useful electrical work. Thermoelectric power generation may occur over a range of temperature regimes, depending on the nature of the heat source. The device can also be operated in reverse by applying a voltage to create a temperature difference through the Peltier effect. Thermoelectric generators, as used in deep-space probes and in gas fuelled generators for remote locations, are extremely reliable but their low efficiencies currently restrict the wider application of the technology.

The efficiency of a thermoelectric device is determined by the materials of which it is composed. Materials' performance[6] may be expressed in terms of a dimensionless figure-of-merit, ZT that is related to the Seebeck coefficient (S), electrical conductivity ($\sigma$) and thermal conductivity ($\kappa$) by $ZT = S^2\sigma T/\kappa$. State-of-the-art commercial thermoelectric modules, with $ZT \approx 1$ at room temperature, consist of alloys of $Bi_2Te_3$. However, as the figure-of-merit falls off rapidly at higher temperatures (Figure 2),[7] $Bi_2Te_3$-related materials are unsuitable for use in power generators. The current materials of choice for such applications are based on PbTe or Si-Ge alloys, both with lower efficiencies than $Bi_2Te_3$.[8] The relatively low efficiency of a thermoelectric generator, relative to mechanical cycles, is thus a significant barrier to wide-scale adoption. It has been suggested[9] that thermoelectric energy recovery cannot compete with large-scale power generation. However, the tremendous opportunities to exploit thermoelectric power generation to extract useful electrical energy from otherwise 'waste' heat in, for example, vehicle exhaust streams or industrial plant, has led to a resurgence of interest in the creation of new high-performance materials.

The fundamental problem in designing new materials for thermoelectric applications lies in the inter-dependence of the three key properties (Figure 3) that determine the figure-of-merit and hence performance. For example, the total thermal conductivity, $\kappa$, has both charge carrier ($\kappa_e$) and phonon ($\kappa_L$) contributions. As $\kappa_e$ is directly related to the electrical conductivity through the Wiedemann-Franz relationship ($\kappa_e = L_0\sigma T$), these two quantities cannot be varied independently. Similarly, high performance requires the unusual combination of a high electrical conductivity ($\sigma$) and low thermal conductivity ($\kappa$); properties which show an opposing dependence on charge-carrier density, whilst a large Seebeck coefficient also requires a high density of states at the Fermi level. Development of high-performance materials therefore requires optimisation of three quantities that cannot be independently controlled in a straightforward manner. As a consequence, research into TE materials has focused on narrow band-gap semiconductors with charge-carrier densities in the range $10^{19}$-$10^{21}$ $cm^{-3}$.

A common approach to improved performance in bulk materials that has been successfully applied is reduction of the lattice contribution, $\kappa_L$, to the thermal conductivity[7] through alloy scattering or by the introduction of 'rattling' atoms (the so-called phonon-glass/electron-crystal approach[10]). More recently, dramatic improvements in performance have been achieved by

exploiting length scale as a variable in the design of materials for thermoelectric applications. In particular, the preparation of materials with critical dimensions in the nanoscale has been shown to produce significant enhancements of the thermoelectric response in known thermoelectric phases over that of the bulk.[11,12] Moreover nanostructuring has led to the development of wholly new systems with unprecedented values of the figure of merit at elevated temperatures.

Key developments in thermoelectric materials have recently been surveyed by Kanatzidis[13,14] and by Snyder and Toberer,[15] whilst progress in understanding the key feature of the influence of interfaces on bulk thermoelectric performance has also been comprehensively reviewed.[16] Here, we focus on recent developments in nanostructuring that have led to significant enhancements in *ZT*.

**Nanostructuring of Thermoelectrics**

The theoretical study of Hicks and Dresselhaus[17] first indicated that low-dimensionality may enhance thermoelectric performance by increasing the Seebeck coefficient, S, over that of the bulk, through quantum confinement effects, providing a means of decoupling S and σ. Reduced dimensionality produces a more highly structured density of states, *N(E)* (Figure 4), than in the conventional bulk phase, potentially leading to sharp changes in *N(E)*. Since S, is related to the derivative of the electronic density of states, *N(E)*, at the Fermi level, through the Mott relation,[18] this affords a means of increasing S and hence ZT. This concept subsequently stimulated considerable efforts to fabricate nanostructures with reduced dimensionality, encompassing quantum wells (2D), quantum wires (1D) and nanodots (0D). Experimental verification of this idea has been achieved experimentally in PbTe quantum wells confined by $Pb_{0.927}Eu_{0.073}Te$ barrier layers for which an estimate of ZT=2 was made (considering only the quantum wells, and neglecting the contribution of the barrier layers).[19] Similarly, Venkatasubramanian and co-workers reported that two-dimensional p-type $Bi_2Te_3/Sb_2Te_3$ superlattices may exhibit ZT values as high as 2.4 at 300 K.[20] However, this performance has yet to be confirmed by other workers. Indeed, one of the major difficulties in working with nanoscale systems is the reliable and reproducible measurement of the three key physical properties, electrical resistivity, thermal conductivity and Seebeck coefficient, in systems where contact resistances and heat losses are appreciable obstacles to accurate measurement.

More recently it has been demonstrated that a substantial reduction in lattice thermal conductivity, $\kappa_L$, over that of the corresponding bulk crystalline phase, is the principal contributor to the enhanced thermoelectric performance of a nanostructured material.[12] This reduction in $\kappa_L$ arises from enhanced phonon scattering by interfaces in a nanoscale system. The different wavelengths in the phonon spectrum of a crystalline solid contribute different amounts to the heat transport. For example in undoped silicon,[21] *ca*. 80% of the heat is carried by phonons with a mean-free-path (mfp) below 10μm and 40% by those with a mfp < 100 nm. Interfaces scatter phonons whose mfp is greater than the spacing between interfaces, the scattering becoming less effective as the mfp is reduced below the interface spacing. Hence interfaces are effective at scattering mid- to long-wavelength phonons, which carry an appreciable fraction of the heat, in contrast with alloy-scattering in which it is primarily the short wavelength phonons that are scattered by substituent atoms. Interfaces also scatter charge carriers and therefore in order to achieve a net increase in the figure-of-merit, it is necessary for interfaces to scatter phonons more strongly than they do electrons. In general this suggests high densities of well-ordered interfaces. However, it has been suggested[11] that it is the interfacial area per unit volume that is the most important factor in reducing the lattice contribution to the thermal conductivity. A further beneficial effect of nanostructuring a bulk material is that interfaces may effectively act as an energy filter.[22] The creation of an energy barrier associated with the interface, can lead to preferential scattering of low-energy charge carriers, thereby increasing the Seebeck coefficient.

The thermoelectric properties of silicon nanowires have attracted the interest of a number of researchers, owing to the large difference in the mfp of electrons and phonons found in this material.[23,24] This makes possible the preparation of nanostructures with one or more dimensions smaller than the mfp of phonons, whilst still larger than those of the charge carriers. This is expected to reduce $\kappa_L$ without affecting the power factor, $S^2\sigma$.[25] Although bulk silicon has a high thermal conductivity at room temperature (*ca.* 150 $Wm^{-1}K^{-1}$), it has been found that the thermal conductivity is reduced by two orders of magnitude in silicon nanowires, and shows a strong dependence on the nanowire diameter.[26] Furthermore, the thermal conductivity of silicon nanowires is also dependent on the surface roughness, with the lattice thermal conductivity of rough nanowires, *ca*. 1.2 $Wm^{-1}K^{-1}$, approaching the amorphous limit for silicon.[24] It has been suggested[24] that the surface roughness plays an important role in screening a broad spectrum of phonons. Recent theoretical calculations are in agreement with these experimental results, and

indicate that the thermal conductivity scales with $(D/\Delta)^2$, where D is the nanowire diameter and $\Delta$ the surface roughness.[27]

Bismuth nanowires have been predicted[28] to have a significantly enhanced Seebeck coefficient, because bulk bismuth is a semimetal, and a semimetal-to-semiconductor transition is expected to occur below a critical nanowire size (*ca.* 50 nm) due to quantum-confinement effects. However, fabrication and measurement of the physical properties of bismuth nanowires is challenging owing to the low melting point of bismuth and the ease of oxidation and fragility of the nanowires: hence, only a limited number of reports on the electrical transport properties of bismuth nanowires are available. Whilst Boukai *et al.* reported small Seebeck coefficients of *ca.* -25 $\mu V\ K^{-1}$ for undoped 72 nm nanowires,[29] Lin and co-workers determined larger values of -48 and -55 $\mu V\ K^{-1}$ for the Seebeck coefficient of wires with diameters of 65 nm and 40 nm respectively. These values are comparable with those of bulk bismuth.[30] More detailed studies of these nanowires are required, particularly an investigation of the effects of nanowire diameter and doping on the Seebeck coefficient and the charge carrier concentration, in order to establish in a conclusive way whether a semimetal-to-semiconductor transition occurs.

**Bulk Nanostructured Thermoelectric Materials**

Whilst the investigations described above have demonstrated the principle that improvements in thermoelectric performance may be realised at the nanoscale, the atomic-scale deposition processes used for the fabrication of quantum dots, nanowires and superlattices are slow, expensive and yield relatively small amounts of material. Such nanostructures may find applications in the cooling of electronic devices - indeed, the first demonstration of a superlattice-based cooling module, integrated into a silicon chip package, has recently been reported[31] - but they are not viable for the fabrication of macroscopic devices for large-scale commercial applications, including those in the field of energy recovery. For this reason, considerable efforts have been expended to develop bulk nanostructured materials, in which the advantages of reduced dimensionality are carried through into a bulk material that can be fabricated in sufficient quantities for large-scale applications. However, the nanostructured form is intrinsically unstable thermodynamically, owing to the high surface free energy. Production of a nanostructured material that retains its nanostructure at the typically high operating temperature of a device, therefore presents a formidable challenge. For example, spontaneous dissolution of

the nanostructures under the operating conditions of the thermoelectric device would lead to degradation of performance as the conventional bulk properties are re-established.

Initially interest focused on production of nanostructured forms of materials with proven thermoelectric performance. Rowe *et al*[32] had demonstrated twenty years ago that the thermoelectric properties of $Si_{80}Ge_{20}$ can be enhanced through grain-size reduction to a few micrometers. For grain sizes smaller than 5 μm, the lattice thermal conductivity is reduced by *ca.* 28% when compared with $\kappa_L$ for the bulk material. Subsequently,[33] it has been shown that the thermal conductivity of n-type $Si_{80}Ge_{20}$ can be further reduced by reducing the grain size to nanoscale dimensions. Ball-milling results in a powder with particles with sizes in the range 30-200 nm, comprised of crystallites of 5-15 nm size. Pronounced boundary scattering of phonons in a hot pressed nanopowder reduces the thermal conductivity by *ca*. 46% to 2.5 W $m^{-1}$ $K^{-1}$, and leads, despite a reduced electron mobility, to an increase in ZT which reaches a maximum of 1.3 at 1173 K; approximately 40% higher than the state-of-the-art bulk material. A similar effect has been reported in the p-type analogue (Table 1).[34]

Recent work[35] has shown that the thermoelectric properties of silicon, whose high thermal conductivity makes the normal bulk form a relatively poor thermoelectric material, can be greatly improved through nanostructuring. In particular, ball-milled n-type silicon, with crystallite sizes in the region of 5-20 nm exhibits dramatic reductions by up to 90% in thermal conductivity over the bulk phase, leading to an improvement in thermoelectric performance by a factor of 3.5 at high temperatures (Table 1). Whilst these findings are similar to those for silicon nanowires,[23,24,26] in this case the enhancement in ZT is observed in bulk nanostructured samples, and the synthetic methodology could be easily scaled up to meet the demands of large-scale applications. Ball-milled PbTe also shows thermopower enhancements that are comparable to those of PbTe/$PbSe_xTe_{1-x}$ quantum dot superlattices.[36] Grain sizes in the range 30 – 50 nm suggest that the effect may be associated with electron filtering rather than modifications to the DOS arising from quantum confinement effects.

Poudel et al[37] have recently demonstrated that ball-milling of bulk p-type $(Bi,Sb)_2Te_3$ in an argon atmosphere, followed by hot pressing, generates a material with thermoelectric properties that are superior to those of the conventional bulk phase. The figure of merit peaks at 373 K where ZT = 1.4. This compares with a value of ZT = 0.9 in the conventional bulk material at the same

temperature. Significantly in the nanostructured material, ZT remains above 0.8 to 523 K, whilst that of the bulk falls to 0.2. Furthermore, no degradation of properties was observed on cycling to 523 K. Careful adjustment of the hot-pressing conditions leaves the interfaces intact, whilst allowing the nanoparticles to fuse, producing a solid that closely approaches theoretical density. The electrical properties are not significantly perturbed by nanostructuring; the power factor being only slightly enhanced above 348 K. The improvement in ZT in the range 293 – 523 K arises principally from a marked reduction of up to 43% in the thermal conductivity. Transmission electron microscopy reveals that the grains are highly crystalline, surrounded by nanometre thick interface regions, and with a wide grain size distribution ranging from a few nanometres to 2 μm.[38] Microscopy also indicates the presence of antimony-rich nanodots and pure tellurium precipitates, 5 to 30 nm in size. The complex microstructure of this material, which, in addition to a wide distribution of grain sizes, also contains a large number of defects, results in scattering of phonons with mfps from the micron to the atomic scale, thereby providing a mechanism to achieve the observed dramatic reductions in thermal conductivity.

Related efforts to exploit nanoparticles to achieve reductions in the thermal conductivity have focused on nanocomposites of materials of proven thermoelectric performance. Such nanocomposites may consist of a single phase, with greatly differing particle sizes, or a mixture of phases, one of which has dimensions in the nanoscale region. For example,[39] hot-pressing $CoSb_3$ powder containing both nano- and micro-scale particles yields a composite with a greatly reduced thermal conductivity, leading, at 700 K, to a 54 % increase in the figure of merit over that of the bulk. Dispersion of $0.1 \leq x/mol\% \leq 1.0$ of SiC in $Bi_2Te_3$ leads to a more modest improvement in ZT at 423 K,[40] although higher SiC contents may offer a means of improving the properties of $Bi_2Te_3$ at higher temperatures.[41]

A strategy that has been applied with great success by Kanatzidis and co-workers[13] is to induce the formation of nanoscale precipitates within a matrix. Materials within the pseudo-binary system $(AgSbTe_2)_x(PbTe)_{1-x}$, exhibit remarkable thermoelectric properties at elevated temperatures.[42] Careful characterisation has revealed that this system is considerably more complex than the solid-solution behaviour, implied by this formalism and the Vegard's law behaviour of the lattice parameters. Partial substitution of lead by a mixture of silver and antimony produces the family $AgPb_mSbTe_{2+m}$ (LAST-m), the phase behaviour of which depends

sensitively on the lead content, m. For materials with m ≤ 8, phase separation occurs, whereas at higher lead contents (m > 10), powder X-ray diffraction data are indicative of the formation of a single-phase. However, careful examination by transmission electron microscopy reveals the presence of (Ag, Sb)-rich nanoinclusions within a PbTe rocksalt matrix (Figure 5).[43] Silver deficiency produces n-type thermoelectrics, with high power factors and a thermal conductivity that is lower than would be expected on the basis of solid-solution behaviour.[42] The nanoinclusions correspond to the endotaxial embedding of regions of one composition inside a matrix of a different composition and preferentially orient along the {001} planes.[44] Remarkably, high-temperature diffraction reveals that the nanoinclusions are thermally stable to at least 800 K.[44] The nanoinclusions appear to scatter acoustic phonons with minimal scattering of charge carriers, with the result that high figures of merit result (ZT = 1.7 at 700 K). Comparable thermoelectric performance has subsequently been observed in samples of $Ag_{0.8}Pb_{18+x}SbTe_{20}$ prepared by mechanochemical alloying followed by spark plasma sintering.[45]

Related systems in which lead is partially substituted by tin (LASTT), [46] or silver is replaced by sodium (SALT-m)[47] exhibit p-type behaviour, with similar compositional inhomogeneities at the nanoscale level, low thermal conductivities and correspondingly high figures of merit. More recently,[48] it has been shown that the analogous $(TlATe_2)_x(PbTe)_{1-x}$ (*A* = Bi, Sb) family of materials, which may be considered as a solid solution between the rocksalt PbTe and ordered rocksalt $TlATe_2$ phases (Figure 6), also possesses thermal conductivities markedly reduced from that of lead telluride and that such phases show promising thermoelectric behaviour. The Bi- and Sb-containing materials exhibit respectively n- and p-type behaviour.

The sensitivity of the LAST-m and related families of materials to the subtleties of microstructure and sample inhomogeneities, result in the properties being critically dependent on the synthesis and processing conditions. Significant variations in the figures of merit for different samples of notionally the same material have been observed. For example, Kosuga *et al*[49] have reported values of ZT as low as 0.2 at 373 K for $Ag_{1-x}Pb_{18}SbTe_{20}$, attributing the reduction from that of the originally-reported materials to microstructural differences. Chen *et al*[50] have also suggested that significant spatial variations in the Seebeck coefficient, arising from multi-phasic behaviour, may contribute to discrepancies in values of ZT obtained for different samples.

Similarly complex behaviour occurs even in the apparently simple ternary rocksalt-type phase $AgSbTe_2$, which exhibits ZT > 1.2 at elevated temperatures. A recent X-ray study[43] has indicated that cation ordering may lead $AgSbTe_2$ to adopt a rhombohedral structure, analogous to that of the ternary thallium-containing phases described above and shown in Figure 6, in place of the originally-proposed[51] cubic rocksalt phase, in which cations are randomly distributed over octahedral sites. It has also been suggested that $AgSbTe_2$ has a complex microstructure, in which $Ag_2Te$ precipitates topotactically and is aligned with a rocksalt matrix of stoichiometry $Ag_{22}Sb_{28}Te_{50.}$ [52]

In a related technique, matrix encapsulation has been used to generate nanoscale inclusions. This methodology exploits the fact that some materials may dissolve in others in the liquid state but not in the solid state. Rapid cooling of a multi-component liquid results in precipitation of an insoluble minority phase, leading to nanoparticles that are embedded in the host matrix of the majority phase. The technique has been applied to nanoprecipitates of Pb, Sb, Bi, and InSb in PbTe. Reductions in thermal conductivity are observed for precipitates of Sb and InSb, whereas Bi appears to lead to an increased thermal conductivity. This may be indicative of the importance of mass contrast between the nanoinclusions and the matrix in achieving reductions in thermal conductivity. Remarkably, the precipitation of *ca*. 2% of antimony in a lead telluride matrix[53] reduces the thermal conductivity by a factor of three to $\kappa$ = 0.8 W $m^{-1}$ $K^{-1}$, the effect being ascribed to enhanced acoustic phonon scattering. When nanoinclusions of lead and antimony are simultaneously present in PbTe, ZT is approximately doubled, reaching a value of 1.5 at *ca*. 700K.[54] This has been ascribed to a simultaneous reduction in thermal conductivity and increase in electron mobility when both lead and antimony are present in the nanoparticles. A similar phenomenon of precipitation of nanoscale particles may also contribute to the thermoelectric performance of $Zn_4Sb_3$, for which evidence of nanoinclusions of Zn has been presented.[55]

An alternative approach to the creation of bulk nanostructured materials is to create grain boundaries consisting of a second phase of nanometre thickness. This may be achieved using hydrothermal methods on seed crystals.[56] Examples of coated nanoparticles include $Pb_{0.75}Sn_{0.25}Se$ on $Pb_{0.75}Sn_{0.25}Te$;[56] $CoSb_3$ on $La_{0.9}CoFe_3Sb_{12}$[57] and alkali metal salt coatings on $(Bi,Sb)_2Te_3$.[58] Changing the interfacial composition in this way produces modest improvements (15-30%) in values of ZT. This is achieved principally through reductions in thermal

conductivity, although some enhancement of the power factor also occurs in the coated $(Bi,Sb)_2Te_3$ phases.[58] The formation of nanocoatings, although little explored to date, offers the potential to effect a high degree of control over the interfacial boundary, to which thermal conductivity in particular appears to be especially sensitive.

## Concluding Remarks

Development of a second generation of nanocomposites will require a more controlled design strategy where the thermoelectric properties of different nanostructures can be predicted and the desired structure created using a bulk procedure.[11,12] This will necessitate the concerted efforts of theoreticians and experimentalists, in order to develop theoretical models that account for the transport properties of such nanocomposites, as well as to develop synthetic methods which enable the preparation of bulk materials with the desired nanostructure.

It has recently been suggested[9] that even with significant gains in efficiency, thermoelectric energy recovery systems will be unable to compete with mechanical generators for large-scale (MW) power generation and that the greatest impact of thermoelectric devices is likely to be in smaller scale (kW) systems, where mechanical engines become less efficient. One such application that is frequently proposed for high-performance thermoelectrics is the recovery of waste heat from vehicle exhaust systems. With over 60 million vehicles manufactured worldwide in 2005 and a forecasted 70 million in 2010, this would represent a high-volume market for thermoelectric products. Sustainability becomes a key issue for implementation of TE technology on this scale. Current niche-market devices are based on Te-containing compounds. As the ninth least abundant element,[59] Te (1 ppb by weight in the earth's crust) is too scarce to support usage on this scale (Figure 7).

After performance, cost of implementation is a major consideration in the development of thermoelectric energy recovery. An upper bound of 12.5 cents per watt has been proposed for thermoelectric power generation modules for automotive applications, for which average vehicle requirements are *ca*. 1 kW of electric power.[60] With current thermoelectric modules requiring 1 kg of thermoelectric material to produce a 1 kW generator, this suggests an upper limit of *ca*. $125 per module; higher efficiencies would of course drive this down. Commodity market data[61] (Table 2) reveal that even if the problem of low efficiency at the operating temperature could be

overcome, raw materials' costs alone would leave little margin for production and fabrication costs for commercial modules based on $Bi_2Te_3$, or on the current material of choice for power generation, PbTe. Consideration of both sustainability and cost issues leads to the conclusion that development of high-performance thermoelectric materials that incorporate more abundant elements such as first-row transition-series elements (Figure 7), is essential to provide a sustainable basis for wide-scale implementation of thermoelectric technology. The discovery of new materials will require an extensive programme of exploratory synthesis, suggesting that there is a key role for materials chemistry in the development of next-generation thermoelectric materials.

## References


1. U.S. Department of Energy. Energy Information Administration. Report# DOE/EIA-0484 (2009) *International Energy Outlook 2009*. Washington: Government Printing Office, 2009.

2. *The Energy Challenge*, Department of Trade and Industry, 2006.

3. C. Liu, F. Li, L.-P. Ma, H.-M. Cheng, *Adv.. Matter.*, 2010, **22**, E28-E62.

4. A.J. Jacobson, *Chem. Mater.*, 2010, **22**, 660-674.

5. M. Gratzel, *Acc. Chem. Res.*, 2009, **42**, 1788-1798.

6. "*Thermoelectrics Handbook: Macro to Nano"*, Ed. D. M. Rowe, Chemical Rubber, Boca Raton, Fl (2006).

7. T.M. Tritt, M.A. Subramanian, *MRS Bulletin*, 2006, **31**, 188-194.

8. C. Wood, *Rep. Prog. Phys.*, 1988, **51**, 459-539.

9. C. B. Vining, *Nature. Mater*., 2009, **8**, 83-85.

10. G. A. Slack, in *CRC Handbook of Thermoelectrics*, Chapter 34, Ed. D. M. Rowe, CRC Press, 1995.

11. M.S. Dresselhaus, G. Chen, M. Y. Tang, R. Yang, H. Lee, D. Wang, Z. Ren, J-P. Fleurial, P. Gogna, *Adv. Matter.*, 2007, **19**, 1043-1053.

12. A.J. Minnich, M.S. Dresselhaus, Z.F. Ren, G. Chen, *Energy Environ. Sci.*, 2009, **2**, 466-479.

13. M.G. Kanatzidis, *Chem. Mater.*, 2010, **22**, 648-659.

14. J.R. Sootsman, D.Y. Chung, M.G. Kanatzidis, *Angew. Chem. Int. Ed.*, 2009, **48**, 8616- 8639.

15. G. J. Snyder, E. S. Toberer, *Nat. Mater.*, 2008, **7**, 105-114.

16. D.L. Medlin, G.J. Snyder, *Curr. Opin Colloid Interface Sci.*, 2009, **14**, 226-235.

17. L. D Hicks, M.S. Dresselhaus, *Phys. Rev. B*, 1993, **47**, 12727-12731.

18. N.F. Mott, E.A. Davis, *Electronic Processes in Non-Crystalline Materials*, Clarendon Press, Oxford, 1979.

19. L. D. Hicks, T. C. Harman, X. Sun, M. S. Dresselhaus, *Phys. Rev. B*, 1996, **53**, R10493-R10496.

20. R. Venkatasubramanian, E. Siivola, T. Colpitts, B. O'Quinn, *Nature*, 2001, **413**, 597-602.

21. A. S. Henry, G. Chen, *J. Comput. Theor. Nanosci.*, 2008, **5**, 141-152.

22. S. V. Faleev, F. Léonard, *Phys Rev. B*, 2008, **77**, 214304.

23. A.I. Boukai, Y. Bunimovich, J. Tahir-Kheli, J.-K. Yu, W.A. Goddard, J. R. Heath, *Nature*, 2008, **451**, 168-171.

24. A. I. Hochbaum, R. Chen, R. Diaz Delgado, W. Liang, E.C. Garnett, M. Najarian, A. Majumdar, P. Yang, *Nature*, 2008, **451**, 163-167.

25. A. Majumdar, *Science*, 2004, **303**, 777-778.

26. D. Li, Y. Wu, P. Kim, L. Shi, P. Yang, A. Majumdar, *Appl. Phys. Lett.*, 2003, **83**, 2934-2936.

27. P. Martin, Z. Aksamija, E. Pop, U. Ravaioli, *Phys. Rev. Let.*, 2009, **102**, 125503.

28. Y. M. Lin, X.Z. Sun, M.S. Dresselhaus, *Phys. Rev. B*, 2000, **62**, 4610-4623.

29. A. Boukai, K. Xu, J. R. Heath, *Adv. Matter.*, 2006, **18**, 864-869.

30. Y. M. Lin, O. Rabin, S.B. Cronin, J.Y. Ying, M.S. Dresselhaus, *Appl. Phys. Lett.*, 2002, **81**, 2403-2405.

31. I. Chowdhury, R. Prasher, K. Lofgreen, G. Chrysler, S. Narasimham, R. Mahajan, D. Koester, R. Alley, R. Venkatasubramanian, *Nature. Nanotech.*, 2009, **4**, 235-238.

32. D.M. Rowe, V.S. Shukla, N. Savvides, *Nature*, 1981, **290**, 765-766.

33. X.W. Wang, H. Lee, Y.C. Lan, G.H. Zhu, G. Joshi, D.Z. Wang, J. Yang, A.J. Muto, M.Y. Tang, J. Klatsky, S. Song, M.S. Dresselhaus, G. Chen, Z.F. Ren, *Appl. Phys. Lett*, 2008, **93**, 193121.

34. G. Joshi, H. Lee, Y. Lan, X. Wang, G. Zhu, D. Wang, R.W. Gould, D.C. Cuff, M.Y. Tang, M.S. Dresselhaus, G. Chen, Z. Ren, *Nano Lett.*, 2008, **8**, 4670-4674.

35. S.K. Bux, R.G. Blair, P.K. Gogna, H. Lee, G. Chen, M.S. Dresselhaus, R.B. Kaner, J-P. Fleurial, *Adv. Func. Mater*, 2009, **19**, 2445-2452.

36. J.P. Heremans, C.M. Thrush, D.T. Morelli, *Phys. Rev. B*, 2004, **70**, 115334.

37. B. Poudel, Q. Hao, Y. Ma, Y. Lan, A. Minnich, B. Yu, X. Yan, D. Wang, A. Muto, D. Vashaee, X. Chen, J. Liu, M.S. Dresselhaus, G. Chen, Z. Ren, *Science*, 2008, **320**, 634-638.

38. Y. Lan, B. Poudel, Y. Ma, D. Wang, M. S. Dresselhaus, G. Chen, Z. Ren, *Nano Lett.*, 2009, **9**, 1419-1422.

39. J.L. Mi, X.B. Zhao, T.J. Zhu, J.P. Tu, *Appl. Phys. Lett*, 2007, **91**, 172116.

40. L-D Zhao, B-P, Zhang, J-F. Li, M. Zhou, W-S. Liu, J. Liu, *J. Alloys Compd.*, 2008, **455**, 259-264.

41. J.F. Li, J. Liu, *Phys. Stat. Sol (a)*, 2006, **203**, 3768-3773.

42. K-F Hsu, S. Loo, F. Guo, W. Chen, J.S. Dyck, C. Uher, T. Hogan, E.K. Polychroniadis, M.G. Kanatzidis, *Science*, 2004, **303**, 818-821.

43. E. Quarez, K.-F. Hsu, R. Pcionek, N. Frangis, E.K. Polychroniadis, M.G. Kanatzidis, *J. Am. Chem. Soc.*, 2005, **127**, 9177-9190.

44. B.A. Cook, M.J. Kramer, J.L. Harringa, M.-K. Han, D.-Y. Chung, M.G. Kanatzidis, *Adv. Func. Matter.* , 2009, **19**, 1254-1259.

45. H. Wang, J-F. Li, W-W Nan, W. Zhou, W. Liu, B-P, Zhang, T. Kita, *Appl. Phys. Lett*, 2006, **88**, 092104.

46. J. Androulakis, K. F. Hsu, R. Pcionek, H. Kong, C. Uher, J. J. D'Angelo, A. Downey, T. Hogan, M. G. Kanatzidis, *Adv. Matter.*, 2006, **18**, 1170-1173.

47. P. F. P. Poudeu, J. D'Angelo, A. D. Downey, J. L. Short, T. P. Hogan, M. G. Kanatzidis, *Angew. Chem. Int. Ed.*, 2006, **45**, 3835-3839.

48. A.V. Powell, F. Guinet, P. Vaqueiro, I.M. Wilcock R.L. Jones, in *Thermoelectric Power Generation*, edited by T.P. Hogan, J. Yang, R. Funahashi, and T. Tritt (*Mater. Res. Soc. Symp. Proc.* Volume 1044, Warrendale, PA, 2008), 343-348.

49. A. Kosuga, M. Uno, K. Kurosaki, S. Yamanaka, *J. Alloys Compd.*, 2005, **391**, 288-291.

50. N. Chen, F. Gascoin, G. J. Snyder, E. Müller, G. Karpinski and C. Stiewe, *Appl. Phys. Lett.*, 2005, **87**, 171903.

51 S. Geller and J.H. Wernick, *Acta. Crystallogr.* 1959, **12**, 46-54.

52. J. D. Sugar, D. L. Medlin, *J. Alloys Compd.*, 2009, **478**, 75-82.

53. J.R. Sootsman, R.J. Pcionek, H.J. Kong, C. Uher, M.G. Kanatzidis, *Chem. Mater.*, 2006, **18**, 4993-4995.

54. J.R. Sootsman, H. Kong, C. Uher, J.J. D'Angelo, C.I. Wu, T.P. Hogan, T. Caillat, M.G. Kanatzidis, *Angew. Chem. Int. Ed*, 2008. **47**, 8618-8622.

55. Ø. Prytz, A. E. Gunnæs, O. B. Karlsen, T. H. Breivik, E. S. Toberer, G. J. Snyder, J. Taftø, *Phil. Mag. Lett.*, 2009, **89**, 362-369.

56. B. Zhang, J. He, X. Ji, T.M. Tritt, A. Kumbhar, *Appl. Phys. Lett*, 2006, **89**, 163114.

57. P.N. Alboni, X. Ji, J. He, N. Gothard, T.M. Tritt, *J. Appl. Phys.*, 2008, **103**, 113707.

58. X. Ji, J. He, Z. Su, N. Gothard, T.M. Tritt, *J. Appl. Phys.*, 2008, **104**, 034907.

59. CRC Handbook of Chemistry and Physics, 87$^{th}$ Edition, Taylor & Francis, Boca Raton, 2006.

60. F.R. Stabler, *Mater. Res. Soc. Symp. Proc.*, 2006, **886**, 13-21.

61. Mineral Commodity Summaries 2009, U.S. Pittsburgh, Government Printing Office, 2009.

**Figure captions**

| | |
|---|---|
| Figure 1 | (a) Schematic representation of a thermoelectric couple, composed of two semiconducting materials; one p-type and other n-type. They are joined at the top by a metal (black bar), to make a junction. When the junction is heated, both types of carriers conduct heat towards the base and power is generated. (b) A commercial thermoelectric module, which contains a number of thermoelectric couples connected electrically in series and thermally in parallel. |
| Figure 2 | Figure of merit shown as a function of temperature for selected thermoelectric materials. (After ref. 7) |
| Figure 3 | Dependence of the Seebeck coefficient (S), electrical conductivity ($\sigma$) and the electronic ($\kappa_e$) and lattice ($\kappa_L$) contributions to the thermal conductivity on the charge carrier concentration n, for a bulk material. (After ref. 8) |
| Figure 4 | Schematic representation of the electronic density of states, *N(E)*, for (a) bulk semiconductor; (b) two-dimensional quantum well; and (c) one-dimensional quantum wire. |
| Figure 5 | A schematic representation of the nanostructure of the $Ag_{1-x}Pb_mSbTe_{m+2}$ phases. |
| Figure 6 | The structural relationship between (a) the cubic rock-salt structure adopted by PbTe (cations, solid circles; anions open circles) and (b) the ordered rock-salt structure proposed for $AgSbTe_2$, in which silver and antimony cations are ordered into successive (111) cation layers (highlighted by shading), resulting in the rhombohedral unit cell outlined in red (silver, black; antimony, magenta; tellurium, white) |
| Figure 7 | Relative abundance of the principal elements in the earth's crust, presented using a logarithmic scale. |

**Table 1: Comparison of maximum ZT values for bulk and nanostructured materials.**

| Material | Bulk | | | Nanostructured | | |
|---|---|---|---|---|---|---|
| | $ZT_{max}$ | Temperature at which $ZT_{max}$ is observed | Ref. | $ZT_{max}$ | Temperature at which $ZT_{max}$ is observed | Ref. |
| Si | 0.2 | 1200 | 35 | 0.7 | 1200 | 35 |
| $Si_{80}Ge_{20}$ (n-type) | 1.0 | 1200 | 8 | 1.3 | 1173 | 33 |
| $Si_{80}Ge_{20}$ (p-type) | 0.7 | 1200 | 8 | 0.95 | 1073 | 34 |
| $(Bi,Sb)_2Te_3$ | 0.9 | 293 | 8 | 1.4 | 373 | 37 |
| $CoSb_3$ | 0.45 | 700 | 39 | 0.71 | 700 | 39 |

**Table 2: Raw materials cost per kg of current and known potential thermoelectric materials. (Based on commodity prices for 2008)[61]**

| Material | $/kg |
|---|---|
| $Bi_2Te_3$ | 118 |
| PbTe | 83 |
| $(AgPb_{18}SbTe_{20})_{0.1}$ | 90 |
| $Si_{0.8}Ge_{0.2}$ | 640 |
| $CoSb_3$ | 11 |
| $La_xCo_4Sb_{12}$ | 11 |
| $La_xFeCo_3Sb_{12}$ | 9 |
| $Yb_{14}MnSb_{11}$ | 820 |

(a)

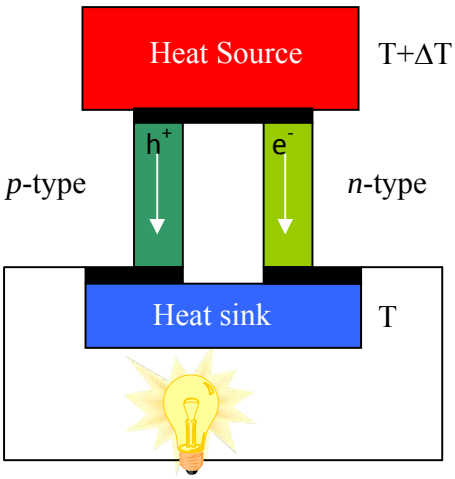


(b)

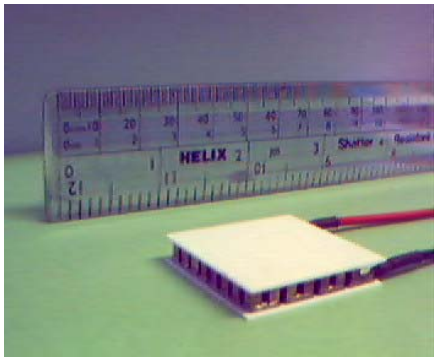

**Figure 1**

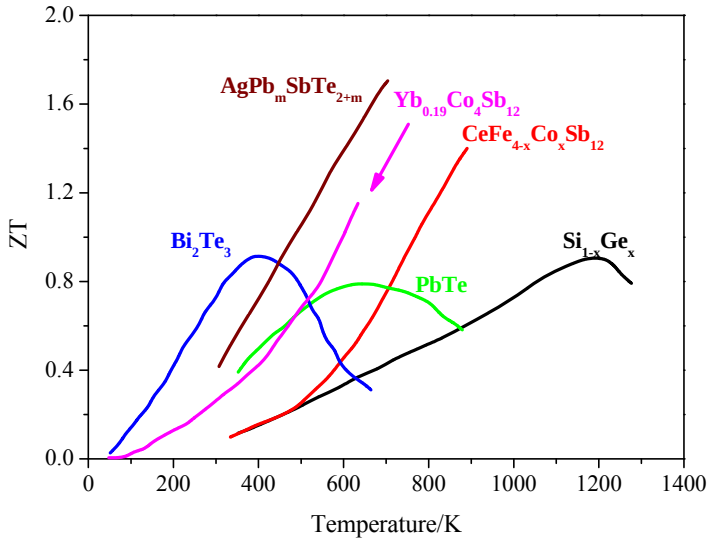
2.0
1.6
1.2
0.8
0.4
0.0
ZT
0
200
400
600
800
1000
1200
1400
Temperature/K
AgPbmSbTe2+m
Yb0.19Co4Sb12
CeFe4-xCoxSb12
Bi2Te3
Si1-xGex
PbTe

**Figure 2**

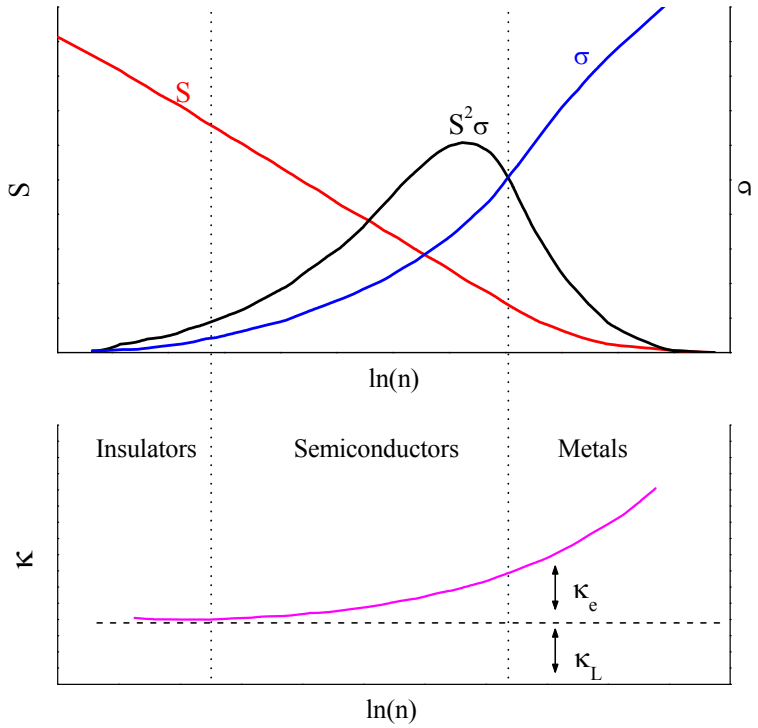


**Figure 3**

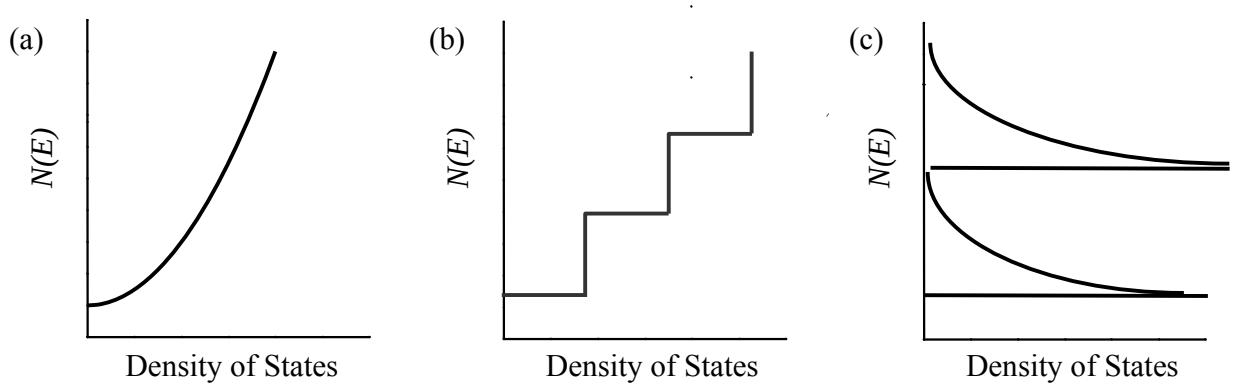
(a)
N(E)
Density of States
(b)
N(E)
Density of States
(c)
N(E)
Density of States

**Figure 4**

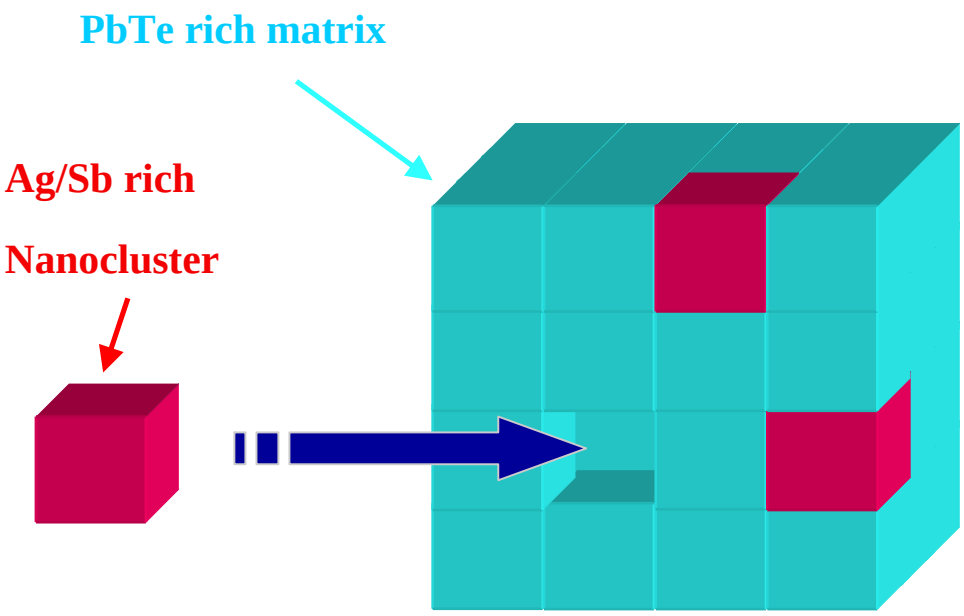


**Figure 5**

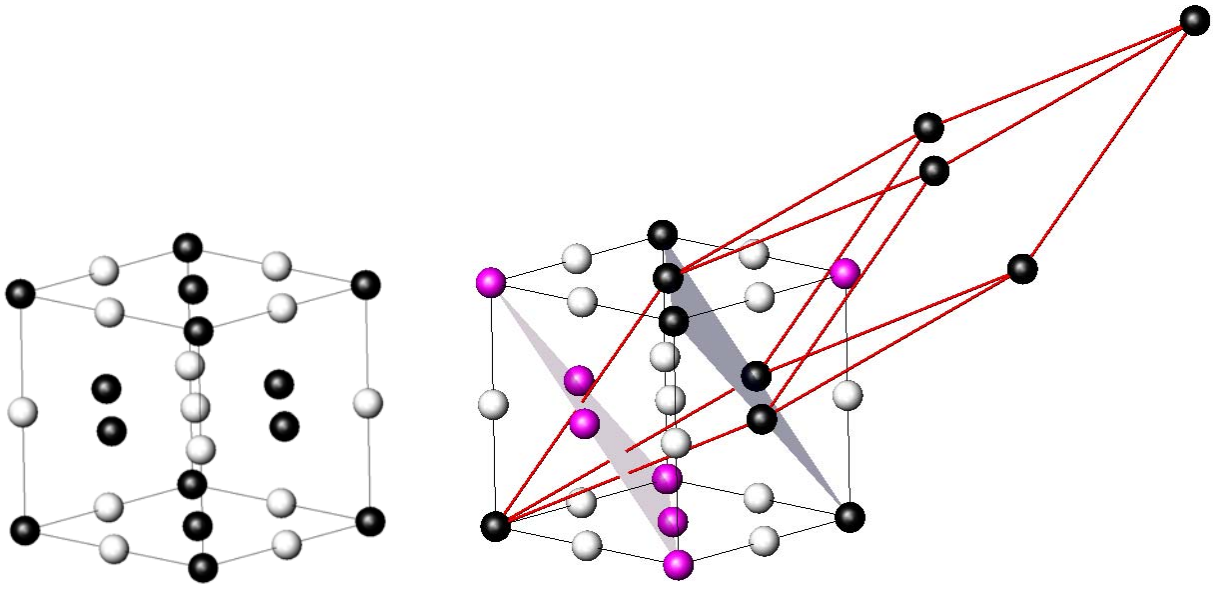

(a) (b)

**Figure 6**

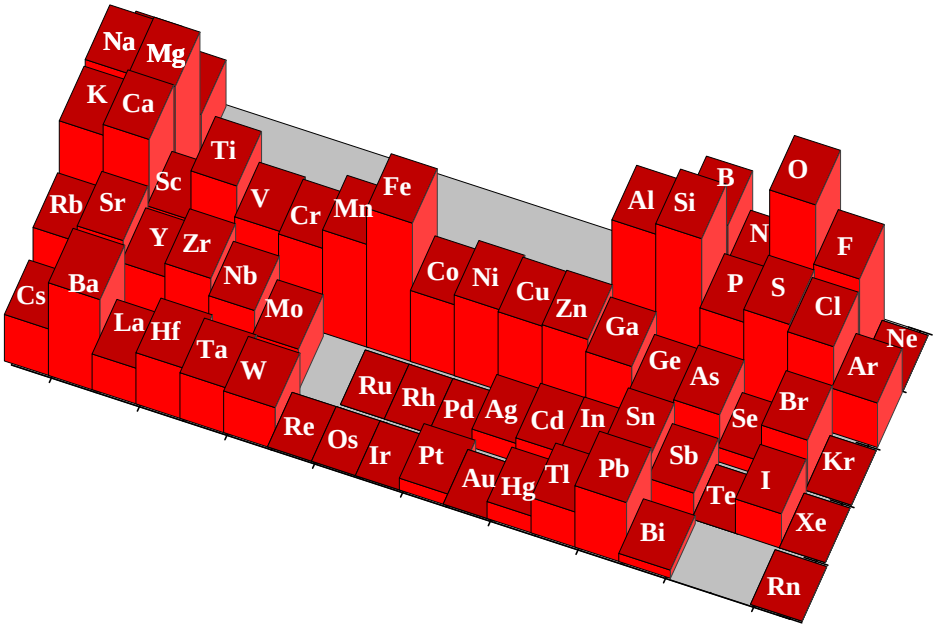
Na
Mg
K
Ca
Ti
Sc
V
Cr
Mn
Fe
Rb
Sr
Y
Zr
Nb
Mo
Cs
Ba
La
Hf
Ta
W
Re
Os
Ir
Pt
Au
Hg
Tl
Pb
Bi
Ru
Rh
Pd
Ag
Cd
In
Sn
Co
Ni
Cu
Zn
Ga
Ge
As
Se
Sb
Te
I
Al
Si
B
O
N
F
P
S
Cl
Ne
Ar
Br
Kr
Xe
Rn

**Figure 7**